Classification of three-photon states in waveguide quantum electrodynamics

Janet Zhong [1,2,*] and Alexander N. Poddubny [1,3]

[1] *Nonlinear Physics Centre, Research School of Physics, Australian National University, Canberra ACT 2601, Australia*

[2] *Department of Applied Physics, Stanford University, Stanford, California 94305, USA*

[3] *Ioffe Institute, St. Petersburg 194021, Russia*

(Received 10 December 2020; accepted 8 February 2021; published 22 February 2021)

We provide the first classification of three-photon eigenstates in a finite periodic array of two-level atoms coupled to a waveguide. We focus on the strongly subwavelength limit and show the hierarchical structure of the eigenstates in the complex plane. The main characteristic eigenstates are explored using entanglement entropy as a distinguishing feature. We show that the rich interplay of order, chaos and localization found in two-photon systems extends naturally to three-photon systems. There also exist interaction-induced localized states unique to three-photon systems such as bound trimers, corner states, and trimer edge states.

DOI: 10.1103/PhysRevA.103.023720

I. INTRODUCTION

A central goal of quantum optics is achieving strong light-matter interactions [1,2]. This can be realized using cavity quantum electrodynamic (QED) platforms or atomic ensembles [3]. A field with growing theoretical and experimental interest is waveguide QED, which is the study of arrays of atoms coupled to a one-dimensional (1D) waveguide. Such systems exhibit collective radiative decay (Dicke super- and subradiance [4]) as well as exotic phenomena unique to the waveguide platform. This includes the fermionization of subradiant states [5,6], bound dimer pairs [7], interaction-induced localization [8], self-induced topological phases [9], and quantum chaos [10]. The important ingredient behind these interesting phenomena is the long-range coupling between atoms found in waveguide QED. It is this that distinguishes waveguide QED from other famous many-body models such as the Bose-Hubbard model, the Heisenberg model, and more which are typically tight-binding models. Waveguide QED is also promising for many applications in quantum information processing. It can allow us to efficiently generate [11–13], detect [14], slow [15], and store quantum light [16]. It is also useful as a platform for quantum simulators of complex many-body physics [17,18]. Experimental waveguide QED platforms can utilize either natural or artificial atoms and examples of existing setups include cold atoms [19], defect centers [20], superconducting qubits [21–27], and emerging structures based on exciton-polaritons [28].

The many-body effects in waveguide QED are mostly unexplored, and rich physics can be expected based on recent theoretical results in the two-photon states [9]. There has been experimental evidence of three-photon bound states (or photonic trimers) in atomic Rydberg setups [29]. Recent theoretical studies have investigated the correlation signatures of a coherent three-photon scattering process in waveguide QED [30], the dynamics of many-body bound states in chiral waveguide QED [31], and the dissipative losses in three-body systems of strongly interacting photons [32]. To our knowledge, there has been no work reporting an overview of eigenstates in the three-photon subspace in waveguide QED. Bound states, where multiple particles are stuck together, are an active area of research in many fields such as ultracold atoms [33]. For clarification, the bound states we investigate are when the photons are bound together but are still free to propagate along the waveguide [7]. This is in contrast to similar studies on atom-photon bound states, where the photon is bound to a lattice site [34,35]. In this paper we extend previous exotic effects in waveguide QED such as fermionization [5], localization [8], bound pairs [7], and chaos [10] to three-photon systems and also predict additional quantum states, requiring at least three photons.

The paper is structured as follows. In Sec. II we describe the waveguide QED Hamiltonian in the three-photon subspace and show the hierarchical composition of the complex energy spectrum. In Sec. III, we focus on the strongly subwavelength regime (where the phase between acquired by light propagating between neighboring qubits is very small at $\varphi = \omega_0 d/c \approx 0.02 \ll 1$) and characterize the main eigenstates using entanglement entropy. In Sec. IV we classify the different types of photon-mediated localization possible in the three-photon subspace. In Sec. V we numerically verify exotic states (corner and three-photon bound states) which occur at slightly larger phase $\varphi = \omega_0 d/c \approx 0.2$ and 1, respectively.

II. MODEL-WAVEGUIDE QED WITH THREE PHOTONS

We consider a finite periodic array of N two-level atoms coupled to a 1D waveguide. Under the Markovian approximation, the effective non-Hermitian Hamiltonian for this system is given by [6,36–38]

$$\mathcal{H} = \sum_{m,n=1}^{N} H_{m,n} b_m^\dagger b_n + \frac{\chi}{2} \sum_{n=1}^{N} b_n^\dagger b_n^\dagger b_n b_n \,, \tag{1}$$

*janet.zhong@anu.edu.au

 ©2021 American Physical Society

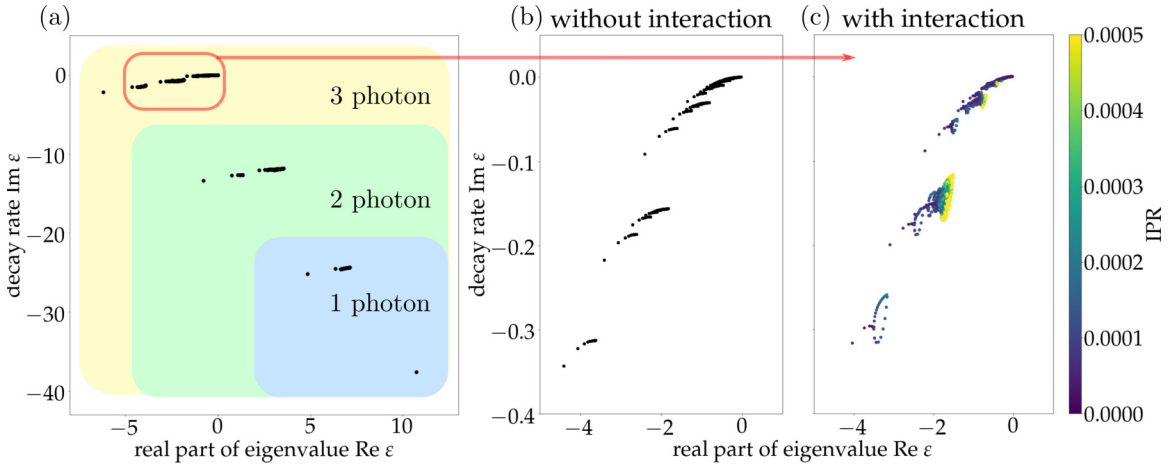

FIG. 1. (a) Full complex energy spectrum of triple excited states for an array of $N = 42$ atoms coupled to the waveguide. (b), (c) Eigenvalues corresponding to the red region in (a) at a zoomed scale with $\chi = 0$ and $\chi \to \infty$, respectively. For (c), the eigenvalues are colored by IPR, where higher IPR means it is more strongly localized. Here, an IPR of 0.0005 indicates that the wave function is localized at around approximately 1–3 lattice sites. The calculation has been performed for $\varphi = 0.02$, $\chi \to \infty$, and the energy is measured in units of $\hbar\Gamma_0$ and counted from the atomic resonance $\hbar\omega_0$.

where the atomic lattice sites are labeled by indices $m, n = 1 \ldots N$ and $H_{mn} \equiv \hbar\omega_0\delta_{mn} - i\hbar\Gamma_0 e^{i\varphi|m-n|}$. Here, b_m are the annihilation operators for the bosonic excitations of the qubits, and $\varphi = \omega_0 d/c$ is the phase acquired by light between the two neighboring qubits, where ω_0 is the atomic resonance of the qubit and d is the qubit spacing. The parameter Γ_0 is the radiative decay rate of an individual qubit. In this system, photons become strongly coupled to atoms and create polaritons, and the χ term represents the on-site polariton-polariton interaction. A single atom cannot be excited twice (termed as photon blockade), and this is represented mathematically by taking the limit $\chi \to \infty$. The imaginary part of the Hamiltonian H_{mn} reflects radiative losses into the waveguide, and there exists long-ranged light-induced coupling between distance atoms described by the term $-i\hbar\Gamma_0 e^{i\varphi|m-n|}$.

Our goal is to understand the main characteristics of the different kinds of the triple-excited states $|\Psi\rangle = \sum \psi_{abc} b_a^\dagger b_b^\dagger b_c^\dagger |0\rangle$. We can obtain the eigenstates and eigenvalues 3ϵ by diagonalizing the Hamiltonian Eq. (1) in the subspace of the Hilbert space with three excitations. Specifically, we construct the effective three-photon Hamiltonian,

$$H^{(abc)} = H^{(a)} \otimes I^{(b)} \otimes I^{(c)} + I^{(a)} \otimes H^{(b)} \otimes I^{(c)} + I^{(a)} \otimes I^{(b)} \otimes H^{(c)}, \tag{2}$$

as a sum of individual Hamiltonians for the first, second, and third photon, which have superscript labels a, b, and c, respectively. This can be written explicitly as

$$H^{(abc)}_{ia,ja;ib,jb;,ic,jc} = \delta_{ib,jb}\delta_{ic,jc}H_{ia,ja} + \delta_{ia,ja}\delta_{ic,jc}H_{ib,jb} + \delta_{ia,ja}\delta_{ib,jb}H_{ic,jc}, \tag{3}$$

where $ia, ja, ib, jb, ic, jc = 1 \ldots N$. The interaction term is

$$U^{(abc)}_{ia,ja;ib,jb;,ic,jc} = (\delta_{ia,ib}\delta_{ja,jb}\delta_{ia,ja} + \delta_{ia,ic}\delta_{ja,jc}\delta_{ia,jc} + \delta_{ib,ic}\delta_{jb,jc}\delta_{ib,jc})\chi. \tag{4}$$

The linear eigenvalue problem to obtain the three-particle excitations is then

$$(H^{(abc)} + \mathcal{U})\Psi = 3\varepsilon\Psi. \tag{5}$$

It is also convenient to transform from the N^3 basis to the $N(N-1)(N-2)/6$ reduced basis where bosonic symmetry and a photon blockade (infinite on-site repulsion $\chi \to \infty$) are already imposed. This can be done using the $N^3 \times N(N-1)(N-2)/6$ transformation matrix B, which is defined as

$$B = [[\tilde{\psi}]_{1,2,3} \quad [\tilde{\psi}]_{1,2,4} \quad \ldots [\tilde{\psi}]_{N-2,N-1,N}], \tag{6}$$

where $[\tilde{\psi}]_{a,b,c}$ cycles through every possible of $a, b, c \in [1, N]$ and $a \neq b \neq c$. Here, $[\tilde{\psi}]_{a,b,c}$ is a column with N^3 elements. The elements ψ_{abc} (and its bosonic symmetry terms) $= \frac{1}{\sqrt{6}}$ and all other elements are 0. We use this reduced basis for all figures in this paper.

In Fig. 1(a), we show the result of numerical calculation of the energy spectrum of a system with $N = 42$ atoms and phase $\varphi = 0.02$ in the three-photon subspace. The eigenvalues are complex because the effective Hamiltonian is non-Hermitian. The imaginary component $\mathrm{Im}(\epsilon) = \Gamma$ of the eigenvalue is the radiative decay rate of the eigenstate. If $|\Gamma| > \Gamma_0 = 1$, where Γ_0 is the radiative decay rate of a single atom, the eigenstates have an enhanced collective decay rate and are *superradiant*. If $|\Gamma| < \Gamma_0$, than the collective radiative decay rate is suppressed and the eigenstates are *subradiant*. The structure of the *noninteracting* three-photon spectra can be reproduced as just the average of three single photon eigenvalues: $\varepsilon \approx (\varepsilon_a + \varepsilon_b + \varepsilon_c)/3$. This means that the structure of the single- and two-photon spectra can be seen within the three-photon spectra, as shown in the green and blue shaded regions in Fig. 1(a). In order to understand the hierarchical structure of the spectrum, we take into account that the single-photon spectrum ε_a becomes denser in the region closer to the atomic resonance $\hbar\omega_0$ due to the low group velocity and high density of states (see also the following discussion of Fig. 3). Hence, if ε_b and ε_c are fixed to some values far from the resonance,

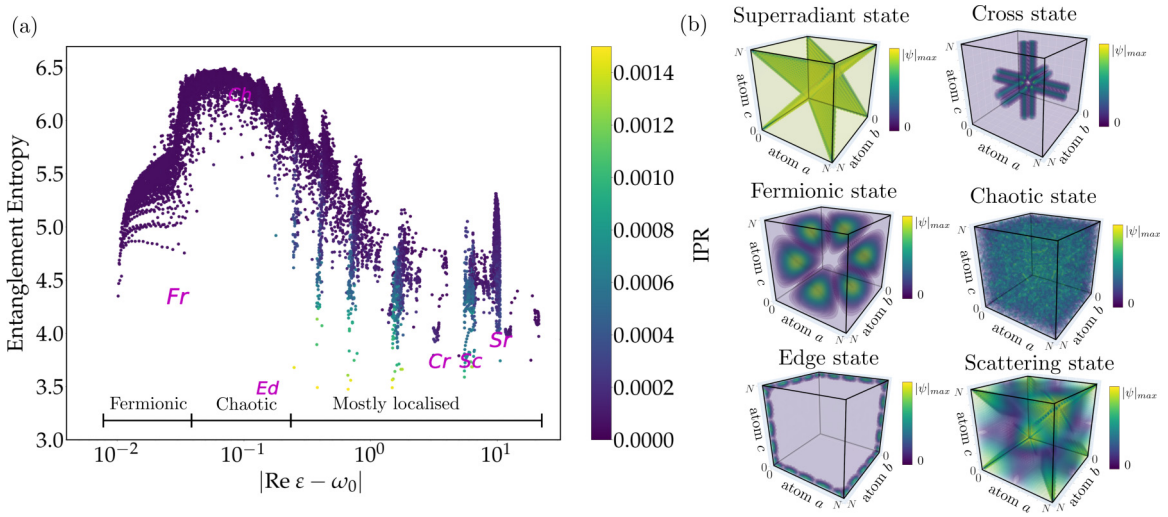

FIG. 2. (a) Entanglement entropy of three-photon states. (b) Characteristic three-photon wave functions of superradiant (Sr), cross (Cr), chaos (Ch), edge (Ed), fermion (Fr), and scattering (Sc) states, which have eigenvalues of $\varepsilon = 10.7298–37.58969i$, $3.5414–11.8320i$, $-0.0727–0.0004i$, $-0.1339–0.0029i$, $-0.010–2.272\times10^{-8}i$ and $-6.182–2.156i$, respectively. Calculation parameters are the same as in Fig. 1.

the variation of ε_a results in a part of the three-photon spectrum that repeats the single-photon spectrum. The calculation demonstrates that the interactions leads to only slight modifications of the energy spectrum as a whole. Figure 1(a) is plotted with infinite on-site repulsion, but on this scale the spectrum looks nearly indiscernible to a noninteracting spectra. Interaction effects become more visible when zooming in, as seen in the comparison between Figs. 1(b) and 1(c), which are plotted without and with interaction, respectively. In Fig. 1(c) the eigenvalues are colored by the inverse participation ratio (IPR) of their corresponding eigenvectors. IPR is defined as

$$\mathrm{IPR} = \frac{\sum_{abc} |\psi_{abc}|^4}{\left(\sum_{abc} |\psi_{abc}|^2\right)^2}, \tag{7}$$

and a high (low) IPR indicates the state is highly localized (delocalized). The high IPR eigenvalues colored yellow in Fig. 1(c) correspond to interaction-induced localized states, which are discussed in more detail in Sec. IV. The cause for the smearing of eigenstates due to interaction is not fully understood but is in line with numerical results from the two-photon case in Ref. [9].

III. CLASSIFICATION OF EIGENSTATES VIA ENTANGLEMENT ENTROPY

The tripartite wave function can be rewritten using the Schmidt decomposition:

$$\psi_{abc} = \sum_{\nu=1}^{N} \lambda_\nu \psi_a^\nu \psi_b^\nu \psi_c^\nu . \tag{8}$$

This is useful because the Schmidt coefficients λ_ν can be used to calculate the von Neumann entropy:

$$S = \frac{-\sum |\lambda_\nu|^2 \ln |\lambda_\nu|^2}{\sum |\lambda_\nu|^2} . \tag{9}$$

It has previously been shown that the von Neumann entanglement entropy is a useful distinguishing feature for the two-photon subspace [9], so we will apply this tool to characterize the main eigenstates of the three-photon case. The entanglement entropy of all eigenstates for a system of $N = 42$ atoms, three photons, and $\omega_0 = 0.02$ is plotted against the rescaled energy $|\mathrm{Re}\,\varepsilon - \omega_0|$ in Fig. 2(a). There are three main "regions," of eigenstates—a fermionic, chaotic, and a mostly localized region. A few characteristic eigenstates are depicted in Fig. 2(b). In these three-dimensional (3D) volume plots, the three axes each show the spatial probability of one photon or polariton along the 1D atomic lattice site index. The probability amplitude is plotted with an opacity of 10%. All eigenstates in the single-photon subspace are standing waves [39]. The three-photon *scattering state* is simply the symmetrized product of three independent standing waves and is very delocalized. These eigenstates can be better understood from examining the single-particle dispersion relation [5] $\varepsilon(k) = \Gamma_0 \sin\varphi/(\cos k - \cos\varphi)$, where k is the Bloch wave vector, so that $\psi_j \propto e^{ikj}$. This polaritonic dispersion has an upper ($k < \varphi$) and lower ($k > \varphi$) branch consisting of an avoided crossing between the photonic dispersion and atomic resonance as depicted in Fig. 3(a). The scattering states are

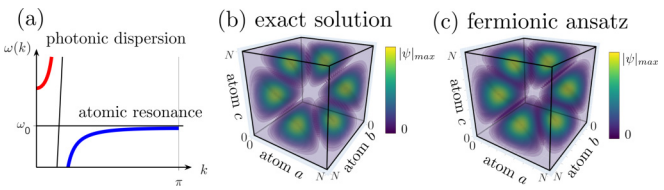

FIG. 3. (a) Polaritonic dispersion relation for waveguide QED system. (b) Fermionic state from exact solution of a system with $N = 42$ atoms, three photons, and $\omega_0 - 0.02$. (c) Fermionic ansatz constructed from antisymmetric combination of three subradiant single-photon eigenstates.

comprised of three photons in the steeper section of the dispersion closer to the photonic dispersion, where k is on the order of φ. A steeper curve means the polariton has a smaller effective mass and larger group velocity. Thus, on-site polaritonic repulsions have less time to take effect, which results in scattering states resembling non interacting eigenstates. It is well approximated by the ansatz that

$$\Psi = c_{123} + c_{321} + c_{213} + c_{312} + c_{132} + c_{231}\,, \tag{10}$$

where we define $c_{123} \equiv u_1(a)u_2(b)u_3(c)$, $c_{213} \equiv u_2(a)u_1(b)u_3(c)$, etc. as shorthand notation where u_1, u_2, u_3 are constituent single-polariton wave functions and a, b, c are the lattice site indices for the three polaritons. For the scattering states they are standing waves or single-polariton eigenstates with different wave vectors.

The *superradiant state* is also a scattering state, but it corresponds to the upper polaritonic branch. The one depicted in Fig. 2(b) has the largest radiative decay rate. The *fermionic state* is the antisymmetric combination of subradiant states and can be described by the ansatz

$$\Psi_{a<b<c} = c_{123} - c_{321} + c_{213} + c_{312} - c_{132} - c_{231}\,. \tag{11}$$

When any of the two particles swap sign, note that Eq. (11) must be multiplied by -1 to preserve bosonic symmetry (the magnitude of the wave function remains unchanged). Here, u_1, u_2, u_3 are again single-polariton eigenstates. The fermionic state can be understood as three polaritons in the flatter region of the polaritonic dispersion closer to $k = 0$ or π. Flatter dispersion means a slower group velocity. This lends more time for interactions to play a role, and the repulsive on-site interaction results in a "Pauli-exclusion" effect [5]. The antisymmetric ansatz is plotted in Fig. 3(c), and it well matches the exact eigenstate depicted in Fig. 3(b).

The *cross states* and the *edge states* are interaction-induced localization states. They are described by an ansatz of the form of Eq. (10), where u_1, u_2, u_3 are either u_{edge}, u_{centre}, or u_{free} depending on the number of photons localized (see Sec. IV for more details). u_{edge}, u_{centre} are single-polariton wave functions localized at the edge or center of the atomic array, respectively, but they are *not* single-particle eigenstates. u_{free} is a free, delocalized standing wave that closely resembles a single-polariton eigenstate. This localization is a phenomena unique to waveguide QED and is caused by light polaritons being trapped in the nodes of the standing waves of heavy polaritons. It can be shown that long-range interactions are crucial for this localization effect [8]. The fact that the localization is interaction-induced distinguishes it from more common localization effects such as Anderson localization.

The *chaotic state* cannot be decomposed into a few single-particle states [10]. It is characterized by a highly irregular wave function in real space and high entanglement entropy, which supports the notion that it is comprised of many entangled single-particle states. Recently, a study on analogous states in two-photon systems [10] shows that they cannot be described using the Bethe ansatz. This suggests that the problem is nonintegrable and exhibits quantum chaos. These chaotic states cannot be described by an equation in the form of Eq. (10).

IV. CLASSIFICATION OF LOCALIZATION

We study the interaction-induced localization in waveguide QED [8] in more detail for a three-photon subspace. A motivating question is how many photons we can have localized in the three-photon subspace. In Fig. 4, we classify the types of localization possible according to whether the photons are localized at the center of the qubit array or at the edge. We numerically verify that we can have combinations of 0, 1, or 2 photons localized at either the edge or the center of the atom array. Note that we can also have localization that is away from the center and the edge. Our ansatz is of the form of Eq. (10):

$$\Psi \approx u_1u_2u_3 + (\text{bosonic symmetry terms}), \tag{12}$$

where u_1, u_2, u_3 are either u_{edge}, u_{centre}, or u_{free}, depending on number of photons localized as according to Fig. 4 (if the photon is not localized it is free), where the bosonic symmetry terms are just the permutations of the first term in Eq. (12). We have manually searched to verify that the maximum number of photons we can have localized in this small subwavelength limit is two photons, as classified in Fig. 4. Having one photon localized corresponds to a plane of high probability amplitude—having two photons localized corresponds to a line, and having three photons localized would correspond to a point in the 3D probability density plot. It may be possible to achieve a situation where all three photons are localized at higher phase, which is briefly mentioned in Sec. V, but eigenstates at higher phase are vastly unexplored even in the two-photon case. In Fig. 4, we also plot a 1D representation of the probability amplitude which we have coined P_a. This is defined as

$$P_a = \sum_{b,c} \psi^2_{abc}, \tag{13}$$

where ψ_{abc} is a component of the three-photon probability amplitude. This just allows us to see where the polariton is localized, as it may be difficult to discern what is happening inside the 3D probability density plots from just the volume plots. We sum the square because otherwise it can sometimes cancel out if parts of the wave function are localized but of opposite parity. We see in this 1D representation that the localization at either the edge or center is quite apparent.

V. EXOTIC STATES AT LARGER DISTANCE BETWEEN ATOMS

In this section we go beyond the strongly subwavelength limit to look for exotic states at higher distance between the atoms, characterized by the phase $\varphi = \omega_0 d/c$. We aim to numerically verify the existence of trimers (three-photon bound state) in waveguide QED systems. Subradiant dimers in the two-photon subspace have been predicted theoretically quite recently, only in 2019 [7]. Photonic trimers were experimentally observed in 2017 in a Rydberg polariton setup and theoretically predicted in waveguide QED systems in Refs. [30,40]. We also numerically verify the existence of several trimer states for the phase $\varphi = 1$. The trimer corresponds to the three photons being bound to each other, which means

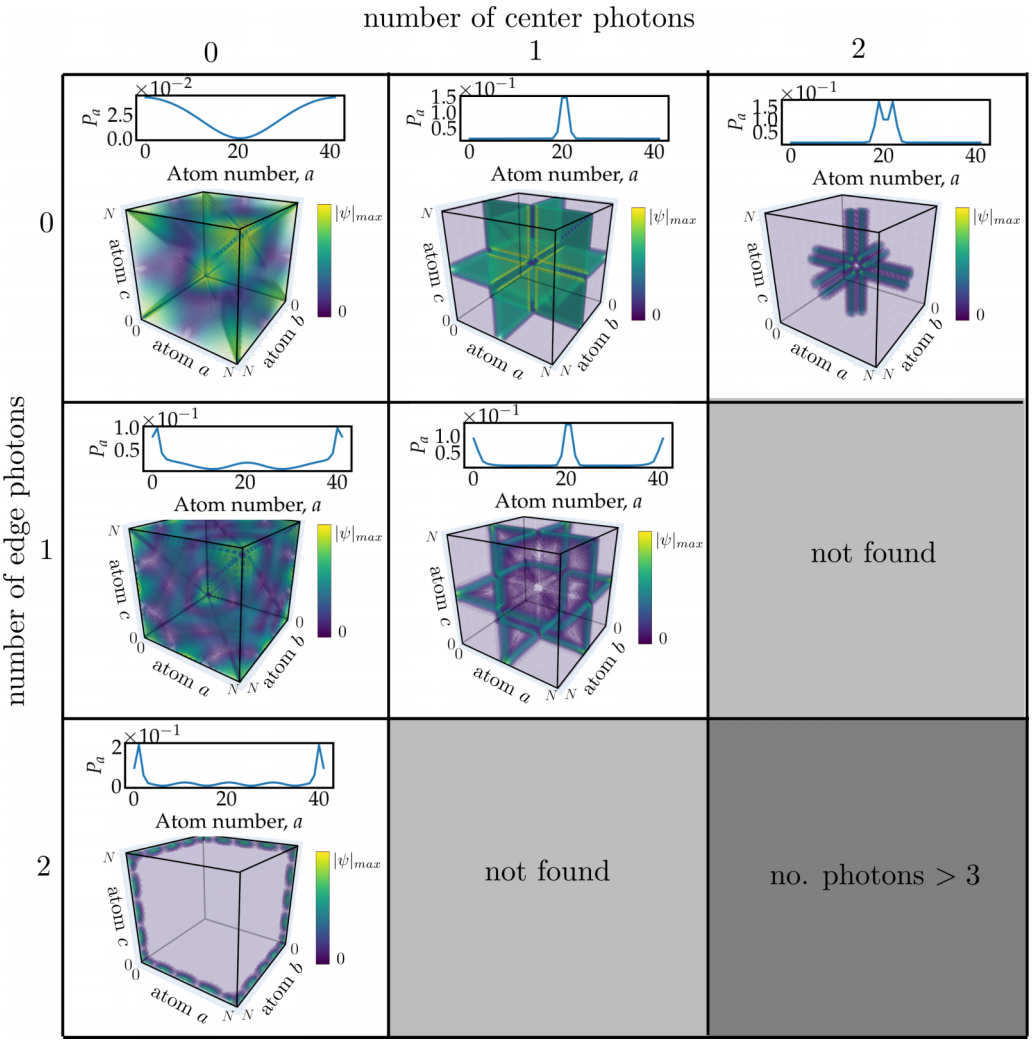

FIG. 4. Classification of the different types of localization possible according to number of photons localized at the edge or center of the qubit array. Above each 3D probability density plot, we show a 1D representation of the probability amplitude defined by P_a as given in Eq. (13). If the sum of photons from the table does not add to 3, then the other photons are free, delocalized photons.

that the probability amplitude exponentially decays from the main diagonal of the 3D probability density plot, as shown in Fig. 5(c).

Unlike the two-photon case, we can also have asymmetrical (relative to the positions in the 1D qubit array) localization for three photons as depicted in Fig. 5(b). With two photons, the standing-wave potential must be symmetrical and our localization can only be symmetrical for a periodic lattice. When the lattice geometry is no longer periodic or symmetrical, we can have asymmetrical localization, as studied in the modulated spaced qubit array in Ref. [41]. In the three-photon case, since we can have overlapping polaritons, this can break the symmetry of the self-induced potential, which allows for asymmetrical localization. The asymmetrical localization also occurs at small phase (such as $\varphi \approx 0.02$ but can become even more prevalent at higher phase. Interestingly, at just a slightly higher phase of $\varphi = 0.2$ we can get corner states, as shown in Fig. 5(a). This is when the photon is exponentially decaying from the edge. This could be related to topological edge states or even higher-order topological edge states, but this is beyond the scope of this paper.

Finally, we also searched for trimer edge states, which is when the three photons are bound together and also localized at the edge. This can be seen as a three-photon extension of the radiative bound pair edge states studied in Ref. [42]. We find some states that satisfy this description at a phase $\varphi = \pi + 0.3$ and plot this in Fig. 5(d). The difference between these states and corner states is that they are exponentially decaying from the main diagonal of the 3D volume plot, whereas corner states exponentially decay along the edges of the volume plot. It is unclear at the moment whether the localization of these trimer edge states has any topological origin. Many exotic effects at higher phase are not understood, even at the two-photon level; however, the very fact that these states exist shows the incredible richness of these waveguide QED systems. We have not yet found dimer states in the three-photon subspace, where only two photons of three are bound to each other.

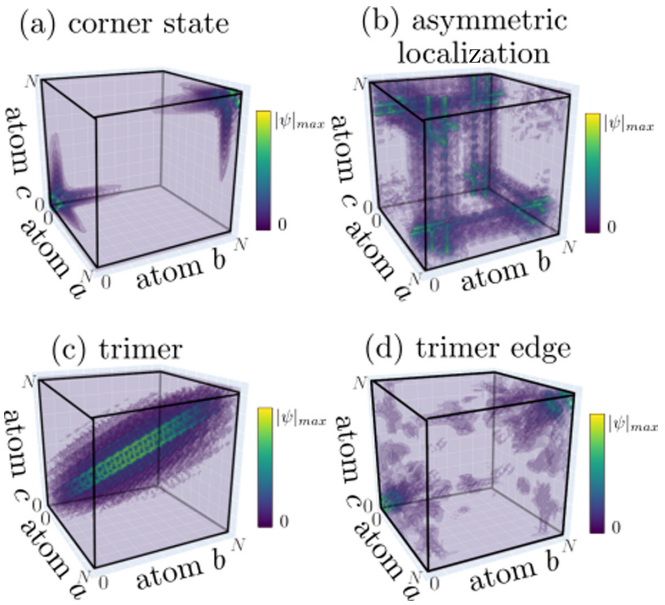

FIG. 5. Exotic three-photon states for larger distance between atoms d. The corresponding phases $\varphi = \omega_0 d/c$ are equal to $\varphi = 1$, $\pi + 0.3$ and 0.2 for the trimer and asymmetric localization, trimer edge and corner state, respectively. Other parameters are the same as in Fig. 1.

VI. SUMMARY AND OUTLOOK

Within this work we give an overview to the broad plethora of states available in the three-photon subspace of waveguide QED systems. We showed the hierarchical structure of the complex eigenstates and broadly classified the main types of eigenstates using entanglement entropy. The fermionic, superradiant, chaotic, and localized states found in two-photon systems [6,8,9] extend quite naturally to the three-photon case. We present a general classification of the possible types of interaction-induced localization possible in the three-photon system. We also numerically verify the existence of exotic states at higher distance between the atoms. Notably, we find bound photonic trimers, which generalizes the subradiant dimers predicted in the two-photon case [7]. Having three photons also breaks the symmetry of the self-induced polaritonic potential, and so we can get asymmetrical localization. Contrary to the systems where the asymmetry is embedded in the lattice geometry [41], here the asymmetry is self-induced by the interactions. Detailed structure of bound trimers requires further studies. For example, it might be useful to calculate their dispersion relations depending on the center-of-mass wave vector, as has been done for the biphoton states in Refs. [7,42]. Our numerical results also indicate a signature of trimer edge states that generalizes bound pair edge states discussed in [42]. Whether these exotic trimer states are relevant to topological edge states or even higher-order topological edge states [43] may be an avenue of future exploration.

ACKNOWLEDGMENTS

This work was supported by the Australian Research Council under Grant No. FT170100331. J.Z. was supported by the Australian Government Research Training Program (RTP) Scholarship. A.N.P. has been partially supported by the Russian Foundation for Basic Research through Grant No. 18-29-20037.

[1] D. Roy, C. M. Wilson, and O. Firstenberg, Rev. Mod. Phys. **89**, 021001 (2017).
[2] D. E. Chang, J. S. Douglas, A. González-Tudela, C.-L. Hung, and H. J. Kimble, Rev. Mod. Phys. **90**, 031002 (2018).
[3] L. Henriet, J. S. Douglas, D. E. Chang, and A. Albrecht, Phys. Rev. A **99**, 023802 (2019).
[4] R. H. Dicke, Phys. Rev. **93**, 99 (1954).
[5] A. Albrecht, L. Henriet, A. Asenjo-Garcia, P. B. Dieterle, O. Painter, and D. E. Chang, New J. Phys. **21**, 025003 (2019).
[6] Y.-X. Zhang and K. Mølmer, Phys. Rev. Lett. **122**, 203605 (2019).
[7] Y.-X. Zhang, C. Yu, and K. Mølmer, Phys. Rev. Res. **2**, 013173 (2020).
[8] J. Zhong, N. A. Olekhno, Y. Ke, A. V. Poshakinskiy, C. Lee, Y. S. Kivshar, and A. N. Poddubny, Phys. Rev. Lett. **124**, 093604 (2020).
[9] A. V. Poshakinskiy, J. Zhong, Y. Ke, N. A. Olekhno, C. Lee, Y. S. Kivshar, and A. N. Poddubny, npj Quantum Inf. **7**, 34 (2021).
[10] A. V. Poshakinskiy, J. Zhong, and A. N. Poddubny, arXiv:2011.11931.
[11] A. González-Tudela, V. Paulisch, H. J. Kimble, and J. I. Cirac, Phys. Rev. Lett. **118**, 213601 (2017).
[12] V. Paulisch, H. J. Kimble, J. I. Cirac, and A. González-Tudela, Phys. Rev. A **97**, 053831 (2018).
[13] X. H. H. Zhang and H. U. Baranger, Phys. Rev. Lett. **122**, 140502 (2019).
[14] D. Malz and J. I. Cirac, Phys. Rev. Res. **2**, 033091 (2020).
[15] J. L. Everett, D. B. Higginbottom, G. T. Campbell, P. K. Lam, and B. C. Buchler, Adv. Quantum Technol. **2**, 1800100 (2019).
[16] P. M. Leung and B. C. Sanders, Phys. Rev. Lett. **109**, 253603 (2012).
[17] I. Buluta and F. Nori, Science **326**, 108 (2009).
[18] I. M. Georgescu, S. Ashhab, and F. Nori, Rev. Mod. Phys. **86**, 153 (2014).
[19] N. V. Corzo, J. Raskop, A. Chandra, A. S. Sheremet, B. Gouraud, and J. Laurat, Nature (London) **566**, 359 (2019).
[20] A. Sipahigil, R. E. Evans, D. D. Sukachev, M. J. Burek, J. Borregaard, M. K. Bhaskar, C. T. Nguyen, J. L. Pacheco, H. A. Atikian, C. Meuwly, R. M. Camacho, F. Jelezko, E. Bielejec, H. Park, M. Lončar, and M. D. Lukin, Science **354**, 847 (2016).
[21] O. Astafiev, A. M. Zagoskin, A. A. Abdumalikov, Y. A. Pashkin, T. Yamamoto, K. Inomata, Y. Nakamura, and J. S. Tsai, Science **327**, 840 (2010).
[22] Z. Wang, H. Li, W. Feng, X. Song, C. Song, W. Liu, Q. Guo, X. Zhang, H. Dong, D. Zheng, H. Wang, and D.-W. Wang, Phys. Rev. Lett. **124**, 013601 (2020).
[23] S. Haroche, M. Brune, and J. M. Raimond, Nat. Phys. **16**, 243 (2020).
[24] A. Browaeys and T. Lahaye, Nat. Phys. **16**, 132 (2020).

[25] A. Blais, S. M. Girvin, and W. D. Oliver, Nat. Phys. **16**, 247 (2020).
[26] A. A. Clerk, K. W. Lehnert, P. Bertet, J. R. Petta, and Y. Nakamura, Nat. Phys. **16**, 257 (2020).
[27] I. Carusotto, A. A. Houck, A. J. Kollár, P. Roushan, D. I. Schuster, and J. Simon, Nat. Phys. **16**, 268 (2020).
[28] S. Ghosh and T. C. H. Liew, npj Quantum Inf. **6**, 16 (2020).
[29] Q.-Y. Liang, A. V. Venkatramani, S. H. Cantu, T. L. Nicholson, M. J. Gullans, A. V. Gorshkov, J. D. Thompson, C. Chin, M. D. Lukin, and V. Vuletić, Science **359**, 783 (2018).
[30] Z. Chen, Y. Zhou, and J.-T. Shen, Opt. Lett. **45**, 2559 (2020).
[31] S. Mahmoodian, G. Calajó, D. E. Chang, K. Hammerer, and A. S. Sørensen, Phys. Rev. X **10**, 031011 (2020).
[32] M. Kalinowski, Y. Wang, P. Bienias, M. J. Gullans, D. P. Ornelas-Huerta, A. N. Craddock, S. L. Rolston, J. V. Porto, H. P. Büchler, and A. V. Gorshkov, arXiv:2010.09772.
[33] K. Winkler, G. Thalhammer, F. Lang, R. Grimm, J. Hecker Denschlag, A. J. Daley, A. Kantian, H. P. Büchler, and P. Zoller, Nature (London) **441**, 853 (2006).
[34] G. Calajó, F. Ciccarello, D. Chang, and P. Rabl, Phys. Rev. A **93**, 033833 (2016).
[35] T. Shi, Y.-H. Wu, A. González-Tudela, and J. I. Cirac, New J. Phys. **20**, 105005 (2018).
[36] Y. Ke, A. V. Poshakinskiy, C. Lee, Y. S. Kivshar, and A. N. Poddubny, Phys. Rev. Lett. **123**, 253601 (2019).
[37] A. Asenjo-Garcia, J. D. Hood, D. E. Chang, and H. J. Kimble, Phys. Rev. A **95**, 033818 (2017).
[38] D. E. Chang, V. Vuletić, and M. D. Lukin, Nat. Photon. **8**, 685 (2014).
[39] T. S. Tsoi and C. K. Law, Phys. Rev. A **78**, 063832 (2008).
[40] Y. Shen and J.-T. Shen, Phys. Rev. A **92**, 033803 (2015).
[41] A. V. Poshakinskiy, A. N. Poddubny, L. Pilozzi, and E. L. Ivchenko, Phys. Rev. Lett. **112**, 107403 (2014).
[42] Y. Ke, J. Zhong, A. V. Poshakinskiy, Y. S. Kivshar, A. N. Poddubny, and C. Lee, Phys. Rev. Res. **2**, 033190 (2020).
[43] F. Schindler, A. M. Cook, M. G. Vergniory, Z. Wang, S. S. P. Parkin, B. A. Bernevig, and T. Neupert, Sci. Adv. **4**, eaat0346 (2018).